Observations of beach cusp morphodynamics on a composite beach

S. J. Pitman[1,2], G. Coco[3], D. E. Hart[2], and J. Shulmeister[2]

[1]School of Geography, Politics and Sociology. Newcastle University, Newcastle Upon Tyne, UK.

[2]School of Earth and Environment. University of Canterbury, Christchurch, New Zealand.

[3]Faculty of Science, University of Auckland, Auckland, New Zealand.

Corresponding author: Sebastian Pitman (seb.pitman@ncl.ac.uk)

Abstract

Substantial volumes of sediment are moved on coarse grained beaches through the formation and destruction of beach cusps, yet the processes governing cusp behaviour remain poorly understood. Here, we combine continuous 2D LiDAR scan data with daily UAV topographic surveys and RGB imagery to provide detailed morphological measurements of beach cusps on a composite beach with the aim to investigate the role of sediment size and tidal stage on cusp behaviour. Rapid changes in cusp height and prominence were observed when storm-eroded gravels were readily transported over relatively impermeable sandy substratum, showing the high-order control that mixed matrix sediments have on this process. Post storm, gravels armoured the swash zone overlaying the sand and were rapidly reworked into horns, with the incipient bays simultaneously experiencing erosion. We provide some of the first field observations to show divergent behaviours occurring simultaneously along the beach as cusps adjust to the new dominant hydrodynamic regime, with some areas experiencing a shortening of cusp wavelength through new horn growth, while others contemporaneously experienced wavelength growth through the removal of intermediate horns. Cusp formation was generally more pronounced on the falling tide, but some evidence indicates horns can also be consolidated and grow in relief at some stages of individual rising tides. This research demonstrates how feedback between sediments, morphology and hydrodynamics are key to determining cusp form, with these insights only made possible through the novel combination of LiDAR, UAV, and camera methods to provide sufficient temporal and spatial resolution to resolve key processes.

Keywords: beach cusps, composite beach, mixed sediment, sand and gravel, LiDAR

1 Introduction

Beach cusps are rhythmic alongshore undulations formed in the swash zone and common on many beach types worldwide. Cusps can be characterized as rounded crescentic embayments (bays) interspersed by raised, shore-normal ridges (horns) with steep lateral relief (Coco et al., 2003; Dodd et al., 2008). They can co-exist at multiple elevations on the shoreface, with their alongshore wavelength and spacing controlled broadly by the cross-shore scale of swash motions (Coco et al., 1999). Cusps have primarily been observed to form as accretional features under low energy, shore-normal ocean wave conditions on reflective beaches (Guest and Hay, 2019; Holland, 1998), but evidence also exists for cusp emergence under erosive conditions from berm erosion (Almar et al., 2008; Otvos, 1964). There continues to be discordance in the literature around the mechanisms responsible for cusp formation, predominantly centred on the theories of standing edge waves (Guza and Inman, 1975), and of self-organisation (Werner and Fink, 1993). Edge wave theory suggests that subharmonic or synchronous edge waves (waves that propagate parallel to the shoreline) create longshore differences in wave run up. The spatial characteristics of these differences in run up are then imprinted onto the beach, resulting in the formation of bays where run up extent is large and horns forming where runup extent is small (Sallenger, 1979). Self-organisation theories focus on the coupling of flow and sediment transport systems, such that localised differences in sediment transport rates can create feedback loops that enable cusps to grow and stabilise (Coco and Murray, 2007). For example, relatively higher elevation areas of the beach would experience more deposition due to reduced swash velocity, and would therefore emerge as horns. Guest and Hay (2019) reflect that there has been a shift in focus from the formation mechanisms towards the morphodynamics of cusps. They highlight the significant gaps in understanding as well as discordant findings regarding several key parameters and factors, such

as the role of grain size, timescales required to build cusps, and the relative roles of erosion and accretion in both the formation and maintenance of cuspate morphologies.

Cusps are commonly observed on coarse grained beaches (Masselink et al., 1997), but do exist across the whole range from sand, to mixed sediment, and pure gravel beaches. The majority of studies have considered cusp morphometry or dynamics on either pure sand (Almar et al., 2008; Holland, 1998; Holland and Holman, 1996; van Gaalen et al., 2011) or gravel (Buscombe and Masselink, 2006; Poate et al., 2014; Sherman et al., 1993) beaches. Mixed sediment beach cusp studies are scarce (exceptions include Nolan et al. (1999)), although this appears to be an area of recent renewed focus (Guest and Hay, 2019; Matsumoto et al., 2020; Pitman et al., 2019a). The colocation of both sand and gravel sediments in the matrix of a mixed sediment beach perhaps makes them some of the most hydrodynamically complex unconsolidated coastlines in the world. As a result, standard process-response models derived from pure sand or gravel beaches elsewhere cannot be applied robustly to mixed sediment environments. Gravel sediments typically require much higher energies to initiate transport than sand sediments, and so the distribution and proportion of sand versus gravel on the beach face is in constant flux (Horn and Walton, 2007). These two sediment fractions are often hydrodynamically sorted and segregated on the beach face. This sorting is prominently displayed in beach cusps (Guest and Hay, 2019), where the coarser fractions of the matrix tend to accumulate on horns while finer sediments converge in the bays, at least at the surface.

Historically, many of the key questions around cusp formation and behaviour remain unanswered due to a lack of sufficient temporal and spatial resolution in the data due to techniques available at the time. The emergence of LiDAR and Uncrewed Aerial Vehicle (UAV) surveys over the last 10 years mean that we are now able to measure beach cusps, and for mixed sediment

beaches the mobility of these two sediments fractions, in more detail than ever before. Historically, key observations of morphodynamic evolution of cusps have relied on either relatively coarse beach profile data, targeting individual horns and bays (Ali et al., 2017; Coco et al., 2003; Masselink, 1999; Nolan et al., 1999), whereas new approaches mean it is possible to collect highly detailed measurements of cusp emergence, spacing, sediment dynamics, and cusp decay at far higher spatial and temporal resolutions (Pitman et al., 2019b). One key area in which these advances have significantly improved our understanding of cusp dynamics is that of video observation. The clear visual signature of beach cusps makes them ideal for long term investigation using coastal imaging cameras, and this has resulted in some of our longest records of cusp behaviour to date (Almar et al., 2008). The key limitation here is that video observations lend themselves best to determining the timescales of construction, merging, and destruction, but they are limited to daylight hours and do not readily provide full 3D topographic information. This means that video observations alone may miss the incipient moments of cusp formation due to either their occurrence at night, or the fact that it takes time for small incipient cusps to develop an obvious visual signature observable in imaging systems. Thus, research gaps remain regarding the details of topographic changes during incipient cusp formation and the role of mixed sediments therein.

Here, we aim to quantify the relative roles of sediment size sorting and tidal processes on beach cusp morphodynamics. We employ high resolution remote sensing techniques to address some of the key gaps identified in the approach of previous studies, and we target a composite beach to better understand the relative role of a mixed sediment matrix in beach cusp behaviour. We provide detailed descriptions and analyses of a series of beach cusp formation, adjustment, destruction, and recovery episodes on a composite beach subject to significant storm wave activity.

2 Data and Methods

2.1 Study site

A 3-week field experiment was conducted on Amberley Beach, Canterbury, New Zealand, between 27th June and 16th July 2021 (Figure 1a). Amberley is a composite beach that is in a long-term erosional state, with approximately 15 m of shoreline retreat over the last 22 years. Gravel components of the beach on the upper foreshore typically have D_{50} = 5.5 mm, and sand on the lower beach face fluctuates between coarse and very coarse (2 mm > D_{50} > 0.5 mm). The beach receives moderate wave energy (mean significant wave period H_s = 2 m, mean peak wave period T_p = 6.5 s) and is micro-to-mesotidal, with an average tidal range of 2 m (Pitman et al., 2019a), and one of the few places globally where perigee-apogee cycles exert more control on the monthly tidal envelope than the spring-neap cycle (Byun and Hart, 2020). The beach often exhibits well developed and dynamic rhythmic beach cusp morphology (Pitman et al., 2019b), with such morphology present along a 50 km stretch of the wider Pegasus Bay coastline. Pegasus Bay beaches grade from accretional sandy beaches in the relatively sheltered south (in the lee of Banks Peninsula), through to composite and then mixed sand gravel beaches along the more exposed northern third of the embayment (Hart et al., 2008).

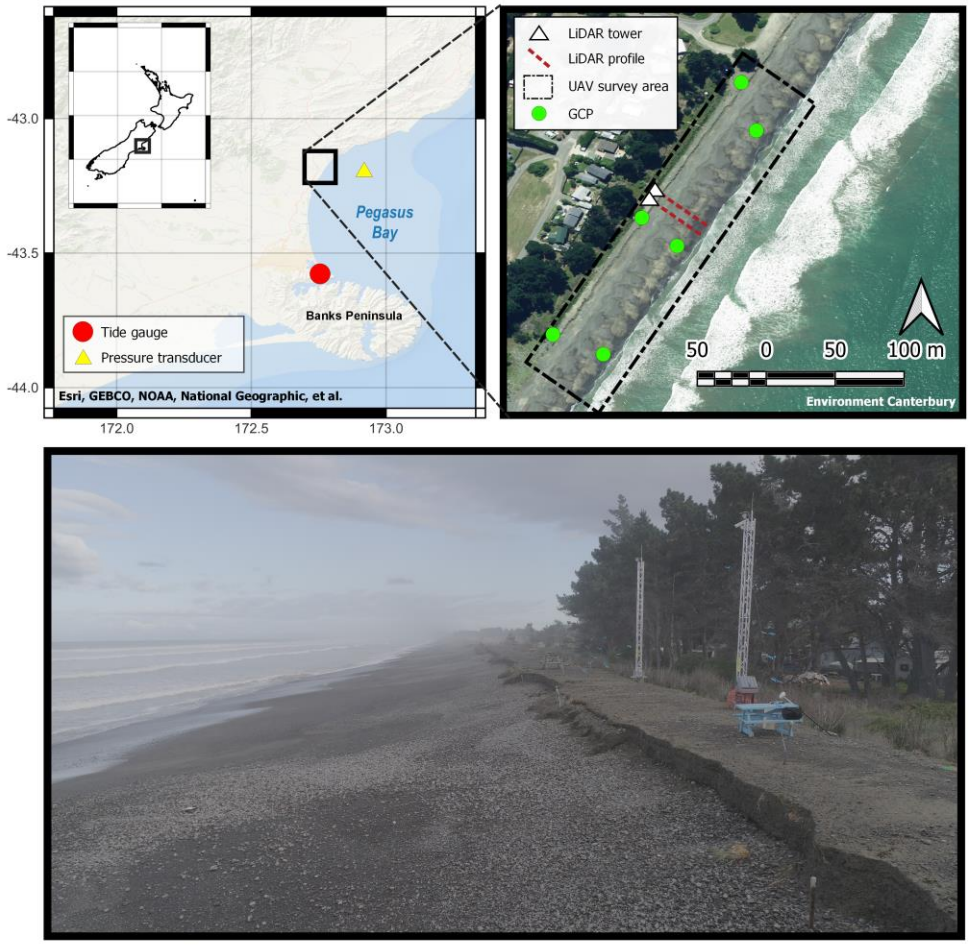

Figure 1. (top left) Amberley Beach is located within Pegasus Bay, New Zealand. A pressure transducer was deployed in 10 m water depth within the bay (yellow triangle) and the Sumner tide gauge (red circle) was used for water levels throughout the study. (top right) Two instrument towers (white triangles) equipped with LiDAR and RGB cameras were deployed within the 300 m UAV survey area, and a typical GCP configuration is shown by green circles. (bottom) Amberley Beach, showing the eroded artificial bund and the instrument towers.

The erosional nature of Amberley Beach, and its proximity to the Amberley Beach settlement means that semi-regular renourishments are undertaken in the form of the construction of an artificial bund at the back of the beach (Figure 1). The nourishment extends 1.2 km along the front of the settlement, is trapezoid in form with a 12 m wide base and a 5 m wide top, built to an elevation around 5 m above mean sea level (MSL). The bund consists of a mixed sand gravel matrix sourced from a quarry pit 800 m from the beach. Resource consent (Environment

Canterbury consent number CRC232136) permits gravels between 5 – 100 mm to be used, with mean gravel size approximately 40 mm. This is coarser than the typical gravel sediment on the upper foreshore (D_{50} = 5.5 mm). The native beach is comprised of around 30% sand according to regional council sediment data, and therefore the nourishment is designed to include up to 25% 'sandy-silt' material to aid cohesion, but no more quantitative measure of sediment size is provided. The construction is largely sacrificial in nature and designed predominantly to prevent overwash events from reaching the low-lying residential development situated only 30 m behind the bund at an elevation roughly equal to the upper beach (approx. 3 m MSL). The bund is now in its fourth iteration, having been progressively retreated over the last 20 years, although the artificially constrained position of the shoreline has resulted in a steeper upper beach profile seaward of the bund compared to on neighbouring less-modified stretches of coastline. The three-week field experiment at Amberley consisted of daily low tide UAV topographic surveys, the deployment of 2 single line scanning LiDAR units, 2 RGB coastal imaging cameras, sediment sampling, and a nearshore pressure transducer, as detailed below.

2.2 Morphodynamic survey

Beach morphology was acquired using the methodology proposed in Pitman et al. (2019b), and was predominantly achieved through daily low tide UAV surveys and Structure from Motion (SfM) techniques. This study used a DJI Phantom 4 Pro quadcopter equipped with a 1" CMOS 20-megapixel RGB camera with a global shutter. The survey targeted a 350 m long and 40 m wide section of beach, acquiring approx. 170 images per survey at a height of 60 m. The quadcopter achieved image overlap of 80% whilst flying at 5 m/s and capturing images on the move. A field of 6 ground control points (GCPs) were laid out, 3 along the top of the renourished bund and 3 as

low as practicable on the beach face and surveyed in using Trimble RTK-GNSS. SfM was conducted using Agisoft Metashape Professional, and was used to create Digital Elevation Models (DEMs) with a horizontal resolution of approximately 0.015 m. Some systematic error was evident in DEMs because of unresolved internal camera parameters, resulting in alongshore curvature of some DEMs. This was corrected using an alongshore-orientated low order polynomial surface which could be corrected back to the linear, horizontal surface of the artificially nourished bund, which provided a static and unchanging reference feature for all surveys. This reduced the RMSE of elevation measurements along the bund from 0.051 m down to 0.025 m. DEMs were then downsampled to a resolution of 0.05 m to aid computational time whilst maintaining sufficient resolution to resolve changes in rhythmic topography. DEMs were filtered using a 1 x 1 m 2D median filter which was useful in removing noise associated with some large woody debris on the beach face after the first storm event. In total 19 such surveys were conducted throughout the 3-week field study.

Two SICK LMS511PRO 2D laser scanners with a maximum scanning range of 80 m (26 m at 10% remission) logging at 25 Hz were deployed atop two 5 m instrument towers located on the bund (Figure 1b) approximately 10 m cross-shore. One tower was initially aligned with the centre of a prominent cusp horn, and the other with the adjacent cusp bay, although these features shifted during the experiment. Due to the low remission achieved on wet dark gravels, the effective maximum range on the scanner was approx. 25 m (equivalent to a cross-shore location of 35 m in the local co-ordinate system) for direct measurement of the bed. The bed was detected at 0.05 m intervals using the low variance method of Almeida et al. (2015), which includes correction of the absolute scanner orientation using a least square error method (Horn, 1987), to match the scanner orientation to the topography derived from the UAV survey (Figure 2a – b). To maximise the

cross-shore extent of topographic information derived from the LiDAR, we use the returns associated with the wave and swash fronts to estimate farfield (typically > 35 m cross-shore) topography. Turbulent water associated with wave breaking and swash motion has a higher remission than sand or dark gravels and is thus detected by the scanner at much greater distances than the bed itself. Such is the coherence of this signal that we can trace it vertically towards the bed to the point at which no further returns are received by the scanner, and we can therefore infer that elevation to be the bed. Given that the point density of the raw laser measurements is sparser at greater distances from the scanner, and the fact that a greater laser beam incidence angle at these locations increases the error, we could not robustly derive bed elevation on a wave-by-wave basis. However, by considering all the measured returns over an extended epoch we can build a more robust estimation of bed level. For each 30-minute window throughout the experiment we construct an extended 1D beach profile based on the minimum elevation returned by the scanner at each cross-shore location over that period. Due to scanner beam divergence at greater distances from the scanner, the minima are calculated over larger bins (0.5 m bins from 30 – 40 m cross-shore, and 1 m bins 40 – 45 m cross-shore). The absolute orientation of this extended minima profile is then corrected using the same rotation matrix that was calculated in the previous step based on the high-accuracy nearfield data. When compared against the daily low tide UAV data, we demonstrate this method to provide a robust estimate of bed elevation at extended distances, with Figure 2d demonstrating that it extends the topographic information derived from the LiDAR out to 50 m cross-shore, compared to just 27 m cross-shore using the low variance bed detection threshold. When considering each low tide survey and accompanying profile for both Tower A and B (a total of 21,600 valid observations), the vertical RMSE between the UAV and the extended LiDAR profile is 0.12 m. When considering Figure 2 we observe that most of the error is associated

with the steep slope transition between the artificially nourished bund and the natural beach at 14 – 16 m cross-shore, therefore, if we recalculate the RMSE to only incorporate values taken from > 16 m cross shore (representing the beach), the RMSE reduces to 0.06 m based on 18,100 valid observations.

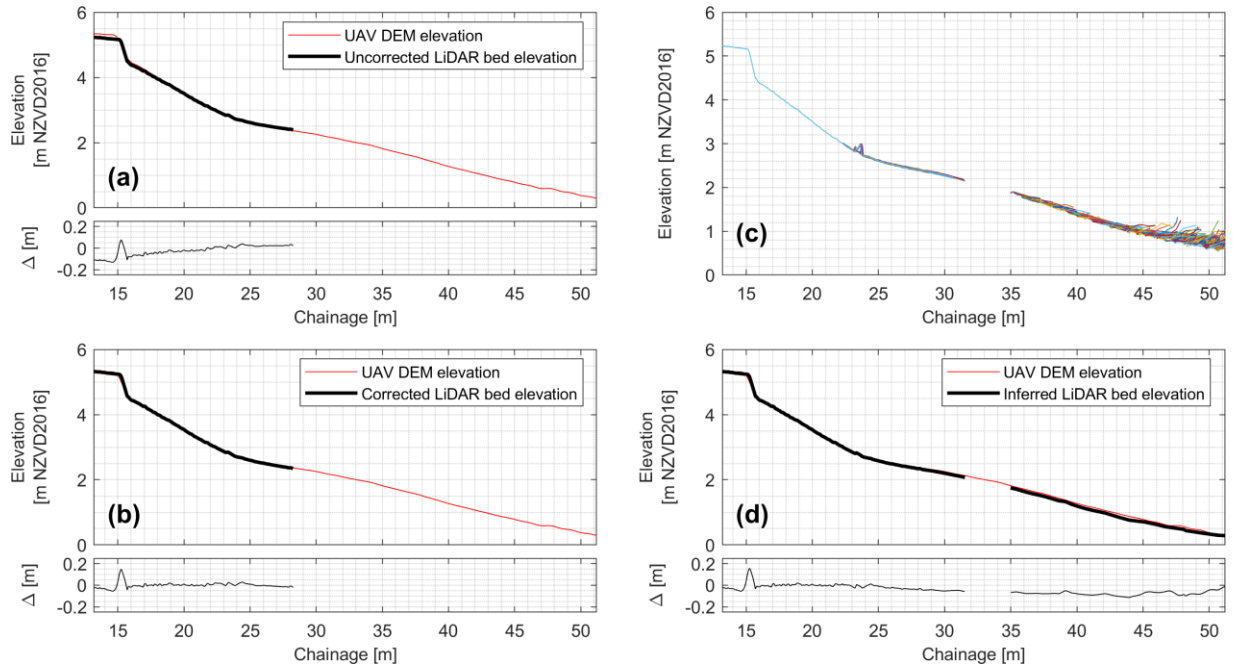

Figure 2. (a) Comparison of UAV derived bed elevation, and that obtained from the LiDAR before orientation correction, with relative error shown below. (b) The corrected LiDAR bed elevation profile following reorientation. (c) All raw LiDAR returns received in the 15 minutes either side of low tide. (d) The extended LiDAR bed elevation inferred from the elevation minima in the raw LiDAR returns.

Two RGB coastal imaging cameras were deployed at the top of Tower 1 (Figure 1b), one orientated cross-shore, and one alongshore to the south. These cameras logged at 4 Hz throughout the study and are useful in qualifying the relative movement of sediments (sand versus gravel) throughout the system. Here we use ‘darkest pixel images’ which are composite images created by saving the single darkest value measured for each pixel over a given sampling period. These images were found to reflect the infiltration signature of the beach face, with darker pixels showing high gravel content due to high infiltration, and lighter pixels indicating lower infiltration rates

where the sand saturation provided a relatively lighter return. These standard coastal imaging products (Holman and Stanley, 2007) were created by applying a 10 minute sample window using images collected at 1 Hz (600 images).

2.3 Hydrodynamics

Tidal elevation was measured by a tide gauge located at Sumner Head, 40 km south of the field site (Figure 3a) which is approximately 9 minutes ahead of tidal stage at the study site (https://tides.niwa.co.nz). Tidal elevation is referenced to NZVD2016 which is 0.41 m below MSL. Nearshore wave conditions were measured using a single RBRsolo^3 deployed in 10 m water depth directly offshore from the field site, and logging at 8 Hz (Figure 3b–d). The study period captured two high energy events, with H_s (significant wave height) peaking at 4 m during a storm over the period 29th June – 3rd July, and between 2 and 3 m over the period 9th – 13th July, with interspersed lower energy periods. $R_{2\%}$ was estimated using Poate et al's. (2016) simplified parameterisation for run up on gravel beaches, given by Equation 1:

$$R_{2\%} = C\ tan\beta^{0.5}\ T_z\ H_s \qquad (1)$$

where C = 0.49, $tan\beta$ represents the average beach slope across both horns and bays, and T_z represents mean wave period.

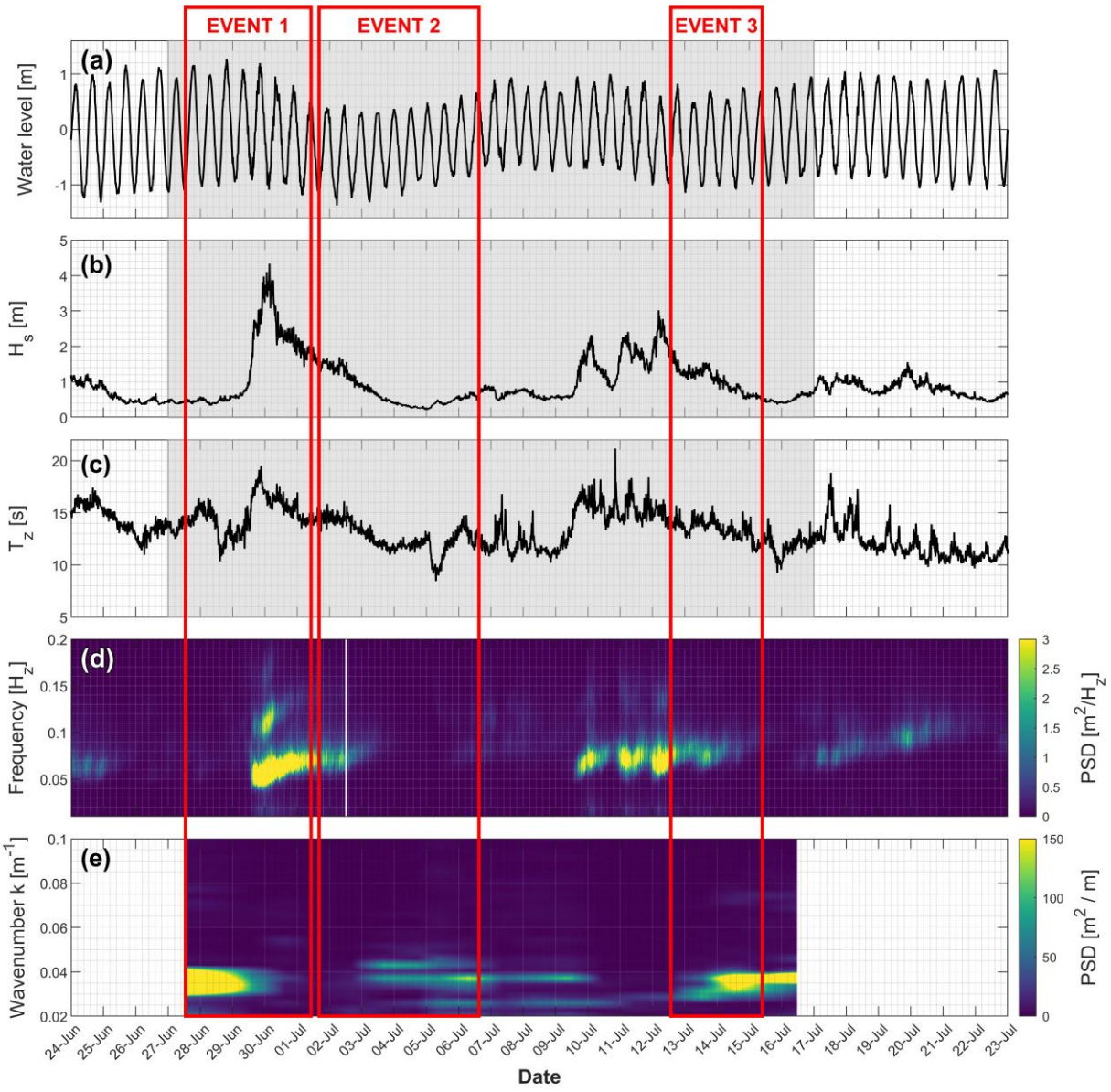

Figure 3. Hydrodynamic conditions measured during the study, including (a) water level from the tide gauge in metres NZVD2016; (b) significant wave height, H_s; (c) mean wave period, T_z; and (d) Power spectrum density (PSD) of the incident wave field. Cusp events were defined by computing the PSD of the alongshore beach contours (e), with PSD > 50 m2 m generally indicative of the presence of cusps. Shading in subplots a – c indicates the deployment duration, and the red boxes highlight Events 1 – 3 which are analysed in further detail in the text.

2.4 Cusp identification

Throughout this paper we adopt cusp descriptors as per the definition of Nolan et al. (1999), such that depth refers to the cross-shore deviation in a given contour, and amplitude refers to the vertical change in elevation alongshore between bays and horns. The presence or absence of beach cusps was ascertained using spectral analysis of the beach contour, following a similar method to that of O'Dea and Brodie (2019). Spectral analysis was conducted on contour lines extracted at 0.5 m elevation increments between 1 m and 3 m elevation (NZVD2016), which is the area of beach face where cusps were observed. For any given survey the contour returning the highest power spectral density (PSD) for a wavenumber between 0.02 and 0.1 m^{-1}, indicative of the largest cusp depth, was recorded and taken as representative of the cusp morphology. These wave numbers represent a cusp spacing between 50 and 10 m, respectively, which is an appropriate bracket for this particular site where cusp spacing is typically between 20 and 35 m (Pitman et al., 2019b). The contour returning the highest PSD was stable over the study period, situated at either 2 or 2.5 m NZVD2016 on 16 of the 19 survey days. The wavenumber corresponding to the largest PSD each day was taken as a measure of mean cusp spacing, and cusps were typically present when PSD values exceeded 50 m^2 m (Figure 3e).

3 Results

3.1 Broad morphological changes

This study captured one cusp destruction event followed by the staged return of cusps over the subsequent fortnight. The timeseries of PSD and wavenumber is a useful means of visualising key changes (Figure 3e). It shows that well developed cusps had a spacing of around 30 m ($k \approx$

0.03), but after storm events during their initial return to the beach face, cusps exhibited spacings of between 20 m (k = 0.05) and 40 m (k = 0.025). Cusps were typically present when PSD values were in excess of 50 m^2 m, with well developed, regularly spaced cusp fields evident when values exceed ~100 $m^2.m^{-1}$. Figure 3e highlights three key events that we examine further below: Event 1 was the removal of cusps as a result of storms activity between 27th June and 1st July; Event 2 was the partial return of cusps to the shoreface between 1st and 6th July; and Event 3 was the return of well-developed cusps between 9th and 14th July.

3.1.1 Event 1: Cusp destruction and rapid re-emergence

At the onset of the experiment on 27th June, prominent well-developed cusps were evident across the profile spanning both upper and lower portions of the beach (Figure 4a), following an extended period of calm wave conditions (H_s < 1 m) and spring tide on 25th June (Figure 3). Energetic storm conditions persisted over the period 27th June – 1st July, with H_s and T_z reaching 4 m and 19 s, respectively (Figure 3). Between 27th – 29th June (Figure 4a – b), the primary profile response was one of erosion. This was initially most prominent on the lower beach cusp horns where elevation changes of 0.5 m were observed, with limited change observed in the elevation of the cusp bays (Figure 4e). This change was accompanied by lower magnitude accretion on the upper beach, dominated by ~0.3 m infilling of cusp bays, and around 0.1 m accretion over upper beach cusp horns. As the storm began to wane, but still under high energy conditions (H_s > 2 m, T_z > 15 s), through 30th June the dominant profile response was accretion (Figure 4f). This was spatially variable, with the emergence of irregular horns low on the beach face, whereas the remaining cusp signature on the upper beach face was removed through a combination of bay

infilling and horn erosion. By 1st July, the beach face was largely planar after erosion of the irregular emergent horns by medium energy ($H_s \approx 2$ m) waves (Figure 4d, g).

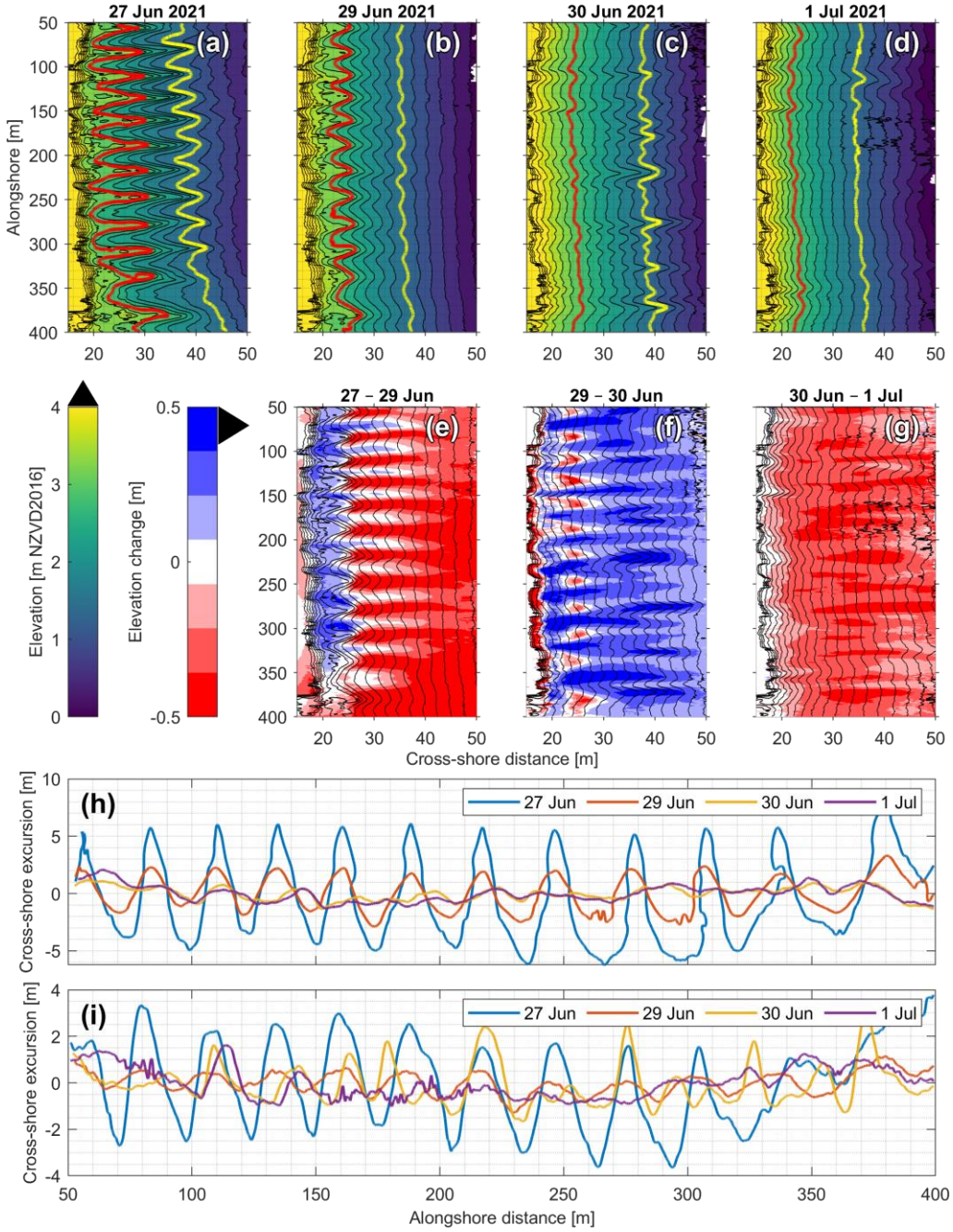

Figure 4. Low tide DEMs from (a) 27th June, (b) 29th June, (c) 30th June, and (d) 1st July 2021, with contours spaced at 0.25 m. The DEMs of difference are shown in panels e – g for the same periods, with the most recent contour lines overlaid. Panel (h) shows the cross-shore excursion

of the upper beach (3 m) elevation contour (the red line in panels a – d), whereas panel (i) shows the cross-shore excursion of the lower beach (1.5 m) elevation contour (the yellow line in panels a – d).

When we examine the beach profile response as recorded by the LiDAR observations, it becomes clear that these changes were strongly linked to tidal stage. Over a 30-hour period between 14:00 on 28 June and 20:30 on 29th June, all the erosion of the prominent upper beach horn occurred during 3 rising tides (Figure 5a – e). On the first rising tide, the toe of the horn was eroded, leading to oversteepening and minor front face collapse (Figure 5a). Despite increasing wave heights, minimal morphological change occurred on the subsequent falling tide. The second flood tide (Figure 5c) eroded the front face of the horn back by 3 m, with vertical bed level changes of around 0.5 m. Minor upper beach erosion was observed in the cusp bay, but both cusp bay and horn experienced up to 0.4 m accretion on the lower beach face. The profile continued to steepen through lower beach face erosion on the ebbing tide. The beach was planed almost entirely flat on the third rising tide, with the horn profile eroded laterally by another 3 m and vertically by 0.5 m (Figure 5e). This was concurrent with infilling of the cusp bays, which experienced accretion of around 0.25 m across the profile.

Orthophoto analysis shows that the removal of horns between 27th and 29th June is associated with an overall fining of surface sediments, resulting in gravel being eroded from the mid beach and by the 29th June constrained to a narrow band at the top of beach above the 2.5 m elevation contour (Figure 6g). When we assess the swash and sediment dynamics using timelapse imagery for the 29th, we observe this distinct separation of sediments on the beachface. The timex imagery shows a wide swash zone (Figure 6b), and offshore inflections at the top of the beach associated with the upper beach cusps. The darkest pixel imagery shows a well-defined hydrodynamic boundary located in the middle of the swash zone (Figure 6a), and based on the

evidence from the drone orthophoto that shows a distinct surface sand - gravel boundary, we interpret this to reflect the two different infiltration regimes associated with surface sand and gravel. The lower beach appears heavily saturated, indicative of low levels of infiltration associated with surface sand. There is then a well defined transition to a darker returns in the upper swash zone which we interpret as areas of high infiltration associated with surface gravel cover. In the initial images for the 29th June where tidal elevations are higher, we see slight inflections in this boundary associated with high tide interactions between swash and upper beach gravelly cusps (Figure 6a, c), however, as the tide elevation falls this becomes an almost linear feature (Figure 6e), the boundary of which bears much closer relationship to the limits of the swash zone evident in the accompanying timex imagery (Figure 6f). Storm conditions peaked on the morning of the 30th June, which on the flood tide (Figure 5g) resulted in accretion across the beach and significant overtopping as observed in the cameras. Wave heights decreased rapidly over the next falling tide, with the result being the prompt return of cuspate morphology to the beach (Figure 5h). For the two LiDAR profiles, this re-emergence was achieved through 0.25 m of horn accretion, and a comparable magnitude of erosion in the neighbouring bay, resulting in an overall cusp amplitude of 0.4 m, with most of the geomorphological adjustment achieved within the first 2.5 hours after high tide. The RGB cameras provide some insight to this process, with analysis of the darkest pixels showing a relatively incoherent spatial distribution of sand and gravel on the beachface (Figure 6h). As tide level falls, we see the rapid return (< 3 hours) of cuspate inflections in the edge of the swash zone in the timex imagery, and the darkest pixel imagery highlights progressively more coherent and cuspate areas of high and low infiltration (Figure 6l). The decrease in infiltration evident in the emergent bays is associated with a fining of material, and the increase in infiltration on the horns is associated with a coarsening. Combining this insight as to

the spatial distributions of sediment during the falling tide (Figure 6) with LiDAR observations that show rapid lower beach horn accretion and bay erosion over this same ~ 3 hour period (Figure 5h), we infer that lateral reworking of sediments into more coherent accumulations of gravel (horns) and sands (bays) is the primary mechanism for cusp re-emergence. The orthophoto at low tide on 30th June (Figure 6n) also provides evidence for the lateral segregation of sediments, with cross-shore orientated accumulations of gravels associated with emergent (albeit irregularly spaced) cusp horns.

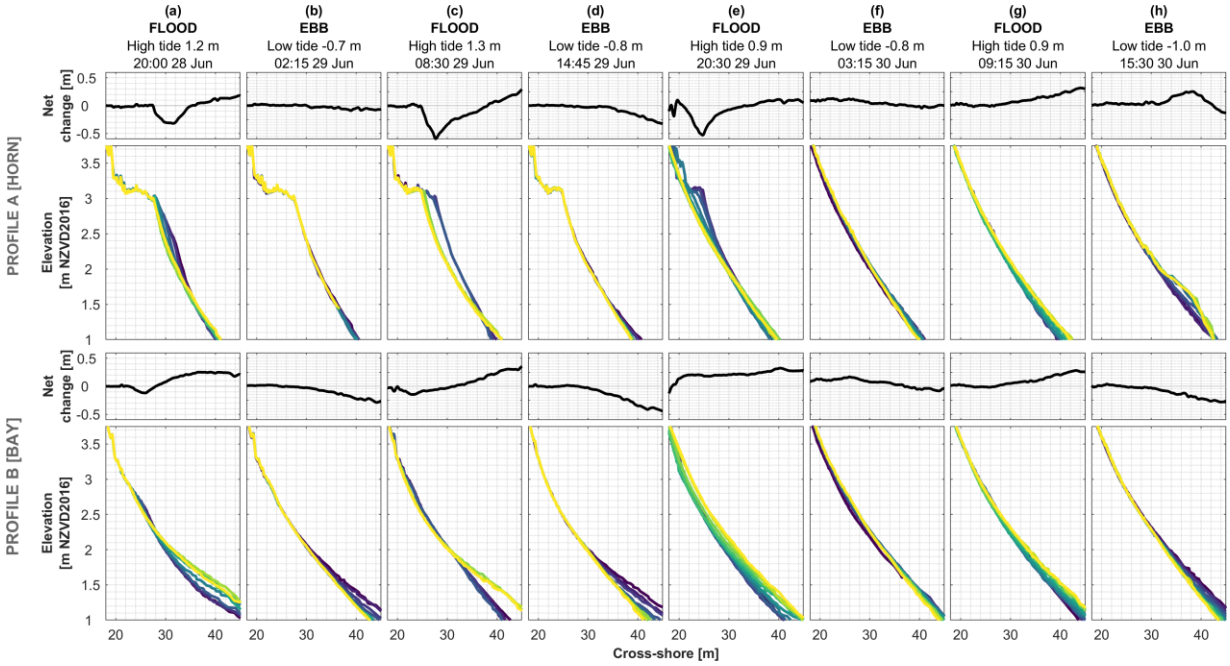

Figure 5. Beach topography change at 30 minute intervals during individual flood and ebb tides between 28th and 30th June. The beach profile change is represented by the individual profile lines, with darker colours (blues) representing the profile at the beginning of the current flood or ebb tide, and lighter colours (yellow and green) representing the profile at the end of that flood or ebb. Net morphological change over the entire tide is shown in the black line above each panel. Profile A represents a LiDAR profile across a well-developed horn in front of Tower 1, and Profile B represents a well-developed bay in front of Tower 2 (Figure 1b).

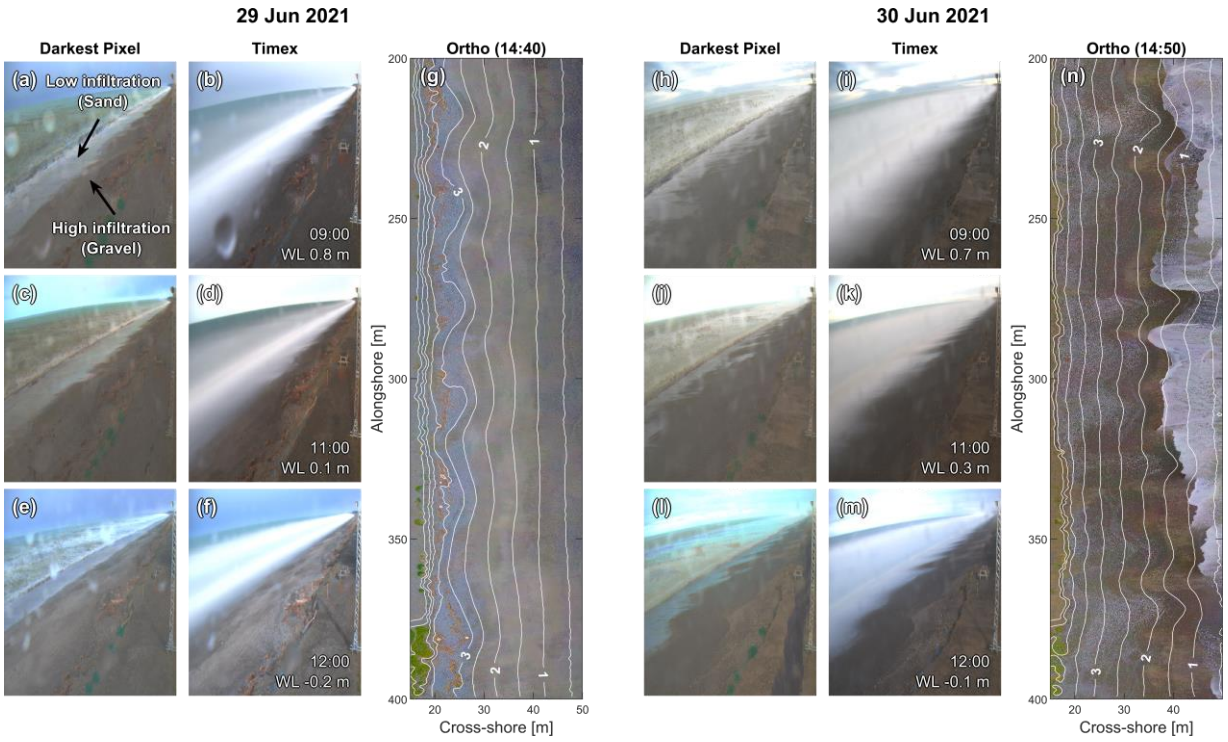

Figure 6. Image products from the RGB monitoring camera located 216 m alongshore, facing south, for the (a – f) 29th and (h – m) 30th June. Darkest pixel products leave a clear signature of infiltration patterns related to sediment composition, and timex products give a broader overview of the width of the swash zone at concurrent times. The orthomosaic derived from the UAV surveys is also presented with beach contour lines and levels in white. Image brightness and contrast are enhanced to visually differentiate gravels from sands (g, n).

3.1.2 Event 2: Cusp merging

As low wave energy conditions (H_s < 1.5 m) persist through to the 6th July a progressive return of beach cusps was evident, first on the lower beach face and latterly at higher elevations (Figure 7). Initially, remnant morphology was exaggerated, with existing areas of positive relief preferentially experiencing accretion, resulting in isolated cusps that displayed atypical rhythmic spacings or forms. This was most prominent between 1st – 2nd July at approximately 110 m alongshore (Figure 7a, b, and e). Over the next 24 hours into 3rd July, accretion on the horns remained the primary control on cusp emergence, with cusps taking a more regular and rhythmic

form across the beach face (Figure 7c, f). These cusps continued to develop through to the 6th July (Figure 7d), with their increased prominence over these final three days due to bay erosion as opposed to horn accretion as earlier observed (Figure 7g). This switch from horn accretion to bay erosion as a mechanism for cusp growth was accompanied by the post-storm decrease in wave energy, with H_s decreasing from around 1.5 m on 1st July to less than 0.6 m over the final three days to the 6th July (Figure 3). When considering the excursion plots, cusp wavelength on the upper beach remained relatively stable over the period (Figure 7h), whereas there was much change on the lower beach face (Figure 7i).

At the start of Event 2, a significant surface covering of gravels existed at all elevations across the beachface, interspersed alongshore infrequently with sand (Figure 8a). On the 2nd July, an isolated horn exists at 110m alongshore, and this correlates to coarser gravel sediments. However, despite the majority of the beachface consisting of gravel surficial sediments, we do not observe horns elsewhere. Through the 3rd – 5th July, we observe a consolidation of gravels on the upper beachface, with sand becoming the dominant surface cover at lower elevations (Figure 8d). This coincides with the emergence of larger and more regularly spaced cuspate morphology. The largest and most prominent horns over this period are associated with coarse deposits, whereas those areas that are more dominated by surficial sand cover (e.g. 200 m alongshore, Figure 8c) exhibit much more dampened cuspate morphology. By 6th July, the cusps are well developed along the entire beach and sandy bays are evident between most horns (Figure 8e).

Cusp development was observed to be non-uniform in different areas of the beach over the same time periods, which was most evident when considering change between the 5th and 6th July (Figure 9). In the northern part of the study area (60 – 240 m alongshore), cusps were initially less well developed than in the southern section. When comparing the change in PSD calculated from

contours in this location, there was a reduction in PSD for k = 0.01 (100 m cusp spacing), and an increase in PSD for k = 0.022 (45 m cusp spacing), showing an overall reduction in wavelength (Figure 9c) as a result of new cusp horns emerging in between the antecedent peaks, effectively halving the wavelength detected. However, in the southern part of the study site the opposite trend appeared, where signal strength also increased around k = 0.022 (Figure 9d), but this was achieved through removal of interspersed horns where k = 0.044 (spacing of 23 m). Therefore, throughout the study area we saw a more rhythmic spacing emerge at about 45 m spacing, but this was differentially achieved through the building new horns and reduction of spacing in the northern section, while in the southern part erosion of horns and increasing wavelengths were observed. This change in spacing occurred as run up (R_2) was estimated to increase from 0.6 to > 1.2 m over the 24-hour period between surveys (Figure 9e).

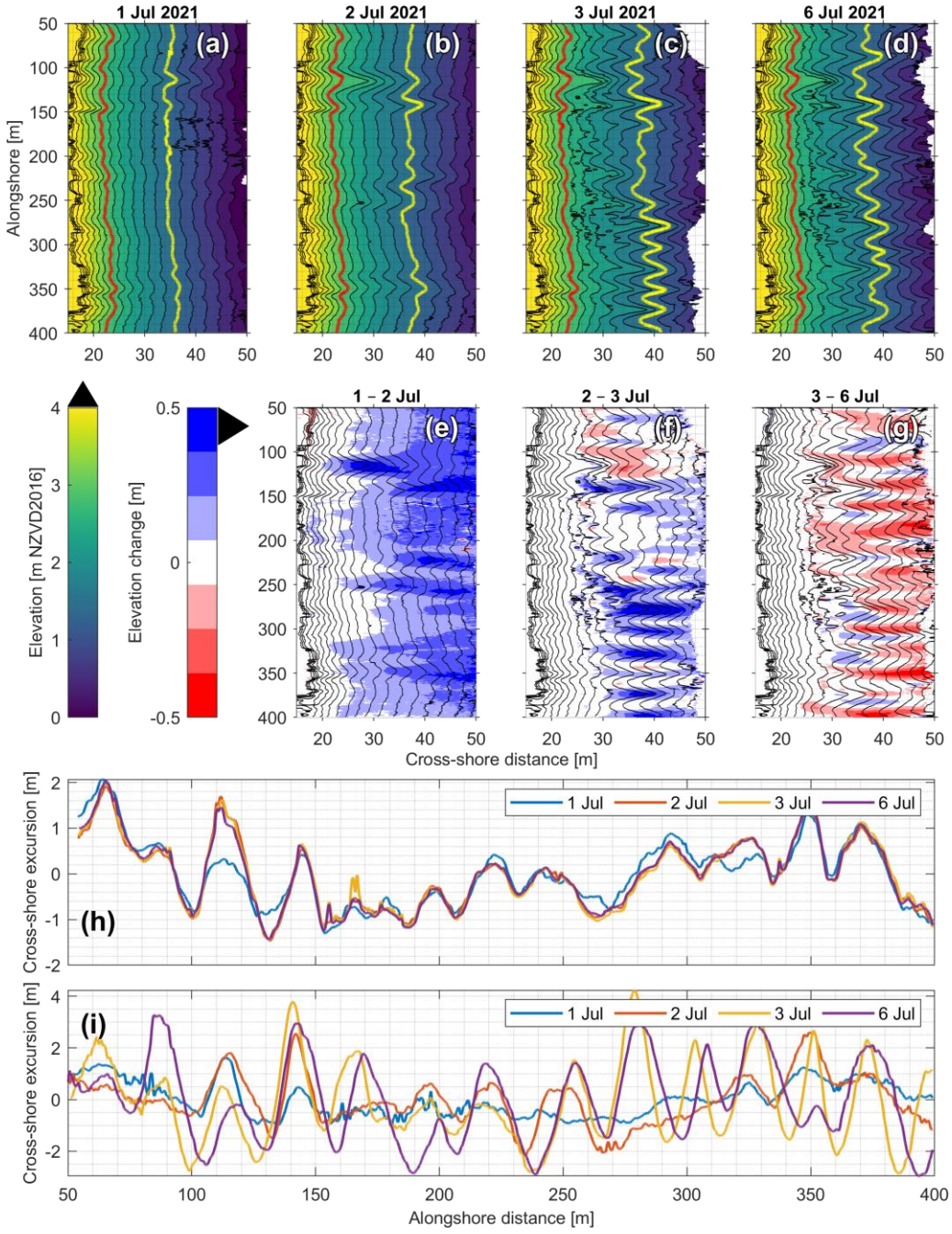

Figure 7. Low tide DEMs from (a) 1st July, (b) 2nd July (c) 3rd July, and (d) 6th July 2021, with contours spaced at 0.25 m. The DEMs of difference are shown in panels e – g for the same periods, with the most recent contour lines overlaid. Panel (h) shows the cross-shore excursion of the upper beach (3 m) elevation contour (the red line in panels a – d), whereas panel (i) shows the cross-shore excursion of the lower beach (1.5 m) elevation contour (the yellow line in panels a – d).

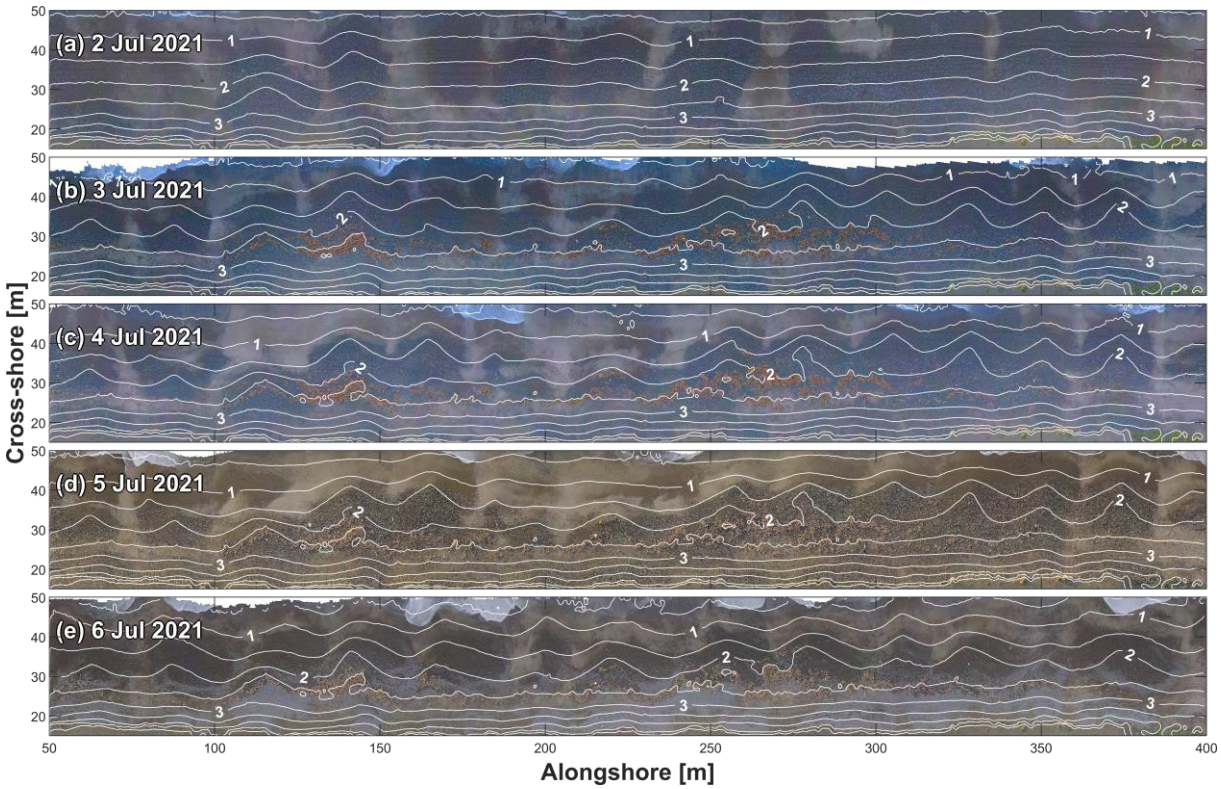

Figure 8. Orthophotos with overlain contours for the period 2nd – 6th July. Gravel sediments are visible as darker patches, with sand showing as lighter areas. Contrast and brightness of the images are adjusted to maximise the visibility of this difference.

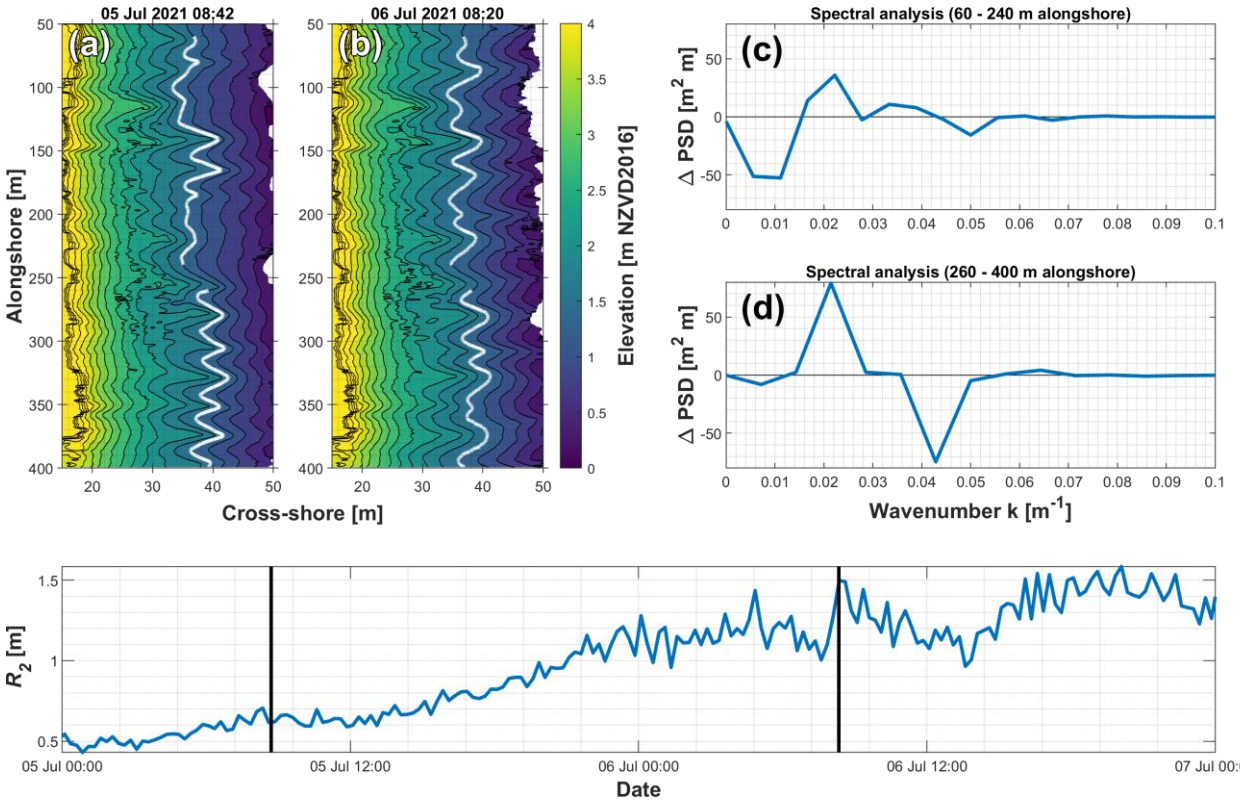

Figure 9. Low tide DEMs from (a) 5th and (b) 6th July with portions of the 1.5 m contour line highlighted in white. PSD was calculated for the 1.5 m contour on both days, and the difference in PSD between both days was plotted for (c) the northern portion (60 – 240 m alongshore), and (d) the southern portion (260 – 400 m alongshore). (e) The 2% exceedance threshold of vertical run up was estimated using Poate et al.'s (2016) runup parameterization, with the two survey periods marked as vertical black lines.

3.1.3 Event 3: Formation of well-developed cusps

As H_s reduced from 2 m to 0.5 m between the 12th – 15th July, we observed the return of well-developed cusps across the beach (Figure 10). Cusp development was initiated via 0.5 m of accretion in the form of emergent horns (Figure 10e), resulting in initial cusp spacing of 34 m (k = 0.029, Figure 3e). Between 13th – 14th July, cusp spacing reduced to 26 m (k = 0.038, Figure 3e) as a result of 0.5 m accretion on new emergent horns between those deposited the day prior (Figure 10f). This process was again not uniform along the beach, with the dominant change occurring in the northern section (60 to 240 m alongshore). In this area, over the 24 hour period between 13th

and 14th July, the PSD associated with 35 m cusp spacing (k = 0.028) reduced by 80 m^2 m, and the PSD associated with 26 m cusp spacing (k = 0.039) increased by 150 m^2 m (Figure 11). This was predominantly achieved through the addition of a brand new horn (approx. 120 m alongshore), and to a lesser degree, the reduction in spacing of cusps to the south of this new horn. Conversely, very little change was observed in the southern part of the beach, other than a slight reduction in the prominence of cusps with a spacing of 28 m (k = 0.036, Δ PSD = - 35 m^2 m). This accretion over the period 12th – 14th July appears to represent a significant proportion of gravel returning to the beach, as evidenced in the different orthomosaics for those surveys (Figure 12g, n). The gravel on the upper beach extended cross-shore by around 10 m during this time, such that by the 14th July it was the dominant sediment at all locations above the 2 m beach contour (down from 2.5 m on the 12th July). The orthomosaic highlights the clear correlation between emergent horn locations and coarser surface sediments (Figure 12n). Finally, bay erosion of between 0.2 m and 0.5 m on the mid and lower beach face between the 14th and 15th July reinforced the existing morphology and increased cusp prominence, with PSD in increasing from 260 to 300 m^2 m (Figure 3e).

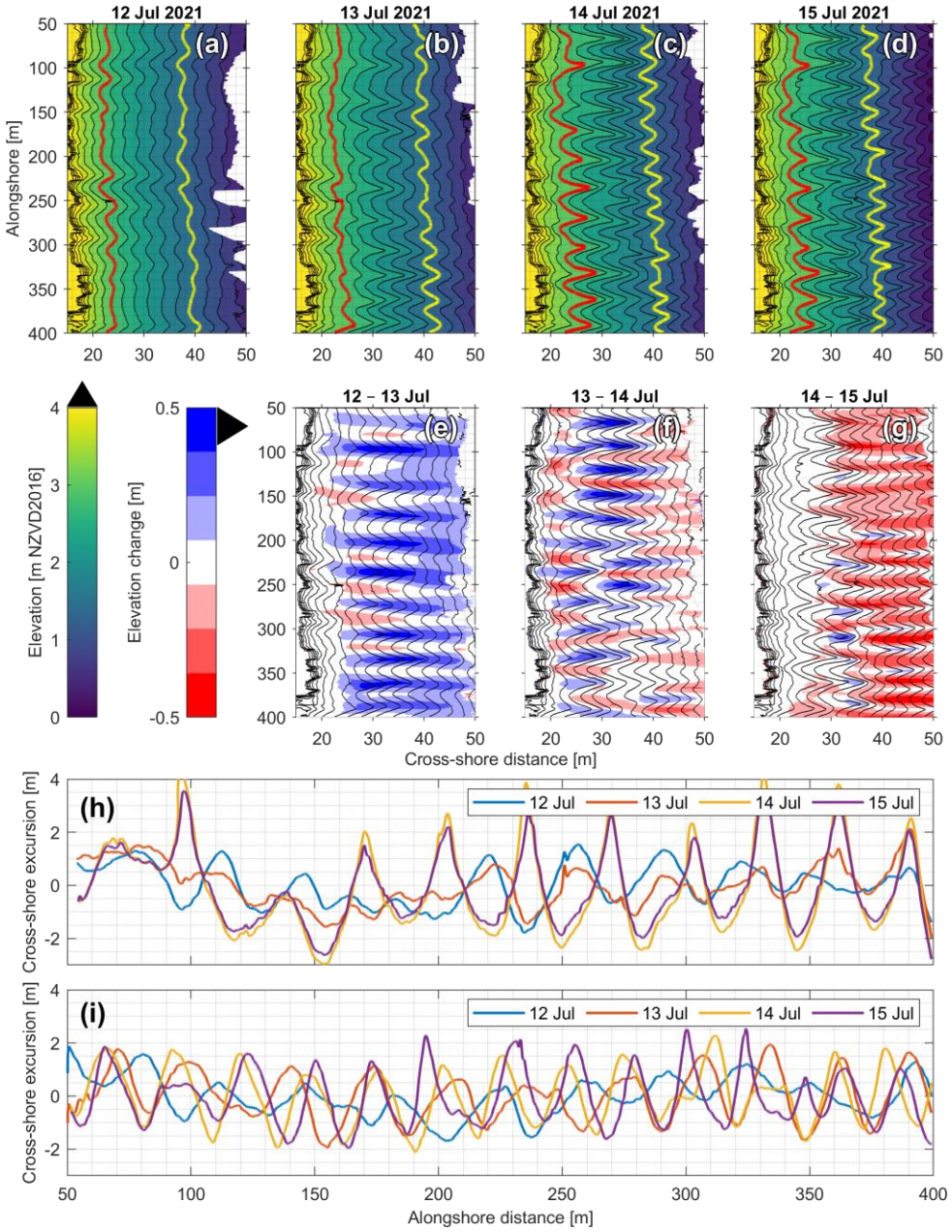

Figure 10. Low tide DEMs from (a) 12th July, (b) 13th July, (c) 14th July, and (d) 15th July 2021, with contours spaced at 0.25 m. DEMs of differences are shown in panels (e – g) for the same periods, with the most recent contour lines overlaid. Panel (h) shows the cross-shore excursion of the upper beach (3 m) elevation contour (the red line in panels a – d), whereas panel (i) shows the cross-shore excursion of the lower beach (1.5 m) elevation contour (the yellow line in panels a – d).

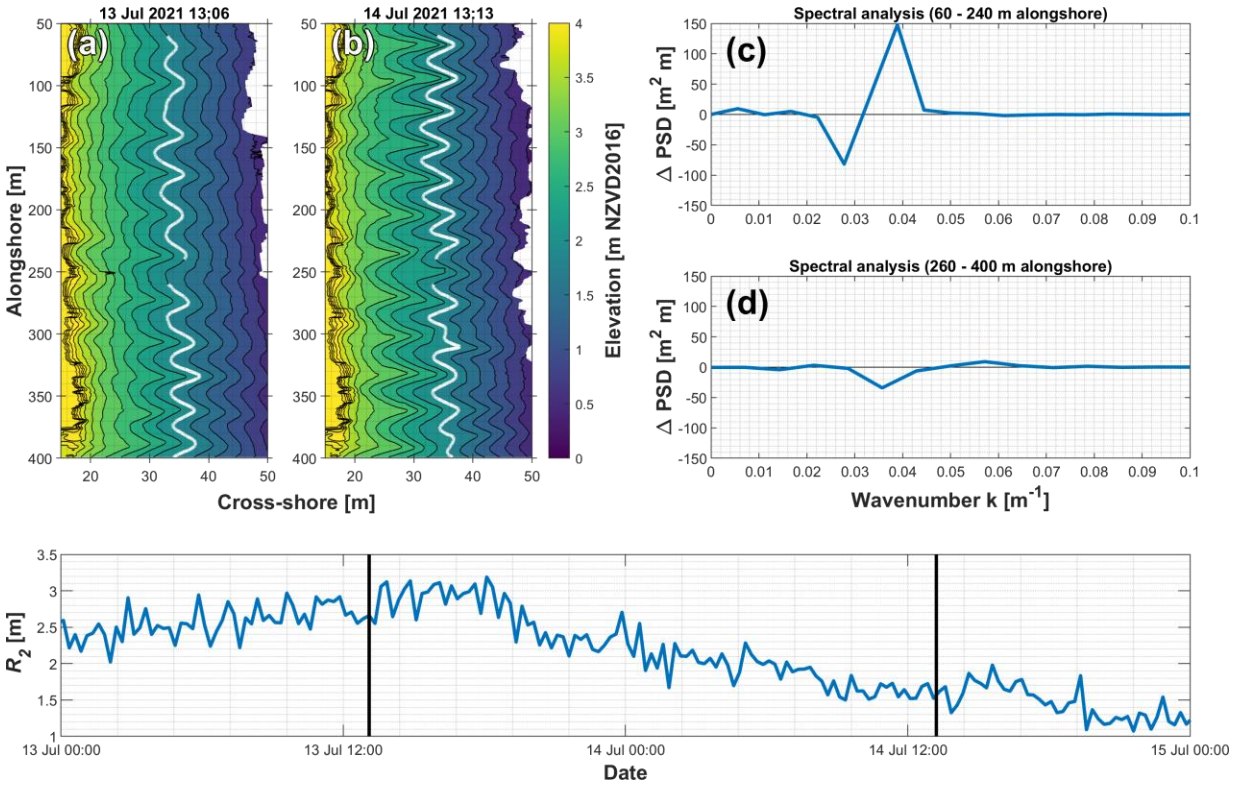

Figure 11. Low tide DEMs from (a) 13th and (b) 14th July with portions of the 2 m contour line highlighted in white. PSD was calculated for the 1.5 m contour on both days, and the difference in PSD between both days was plotted for (c) the northern portion (60 – 240 m alongshore), and (d) the southern portion (260 – 400 m alongshore). (e) The 2% exceedance threshold of vertical run up was estimated using Poate et al.'s (2016) runup parameterization, with the two survey periods marked as vertical black lines.

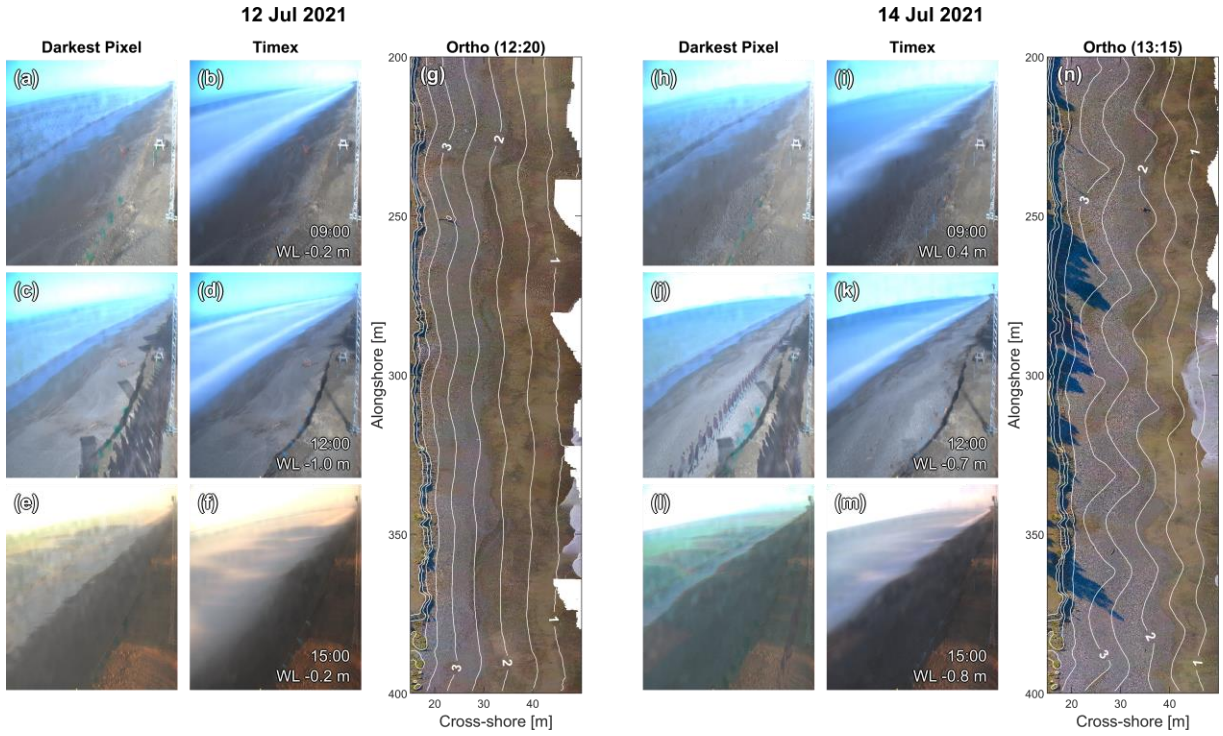

Figure 12. Image products from the RGB monitoring camera located 216 m alongshore, facing south, for the (a – f) 12th and (h – m) 14th July. The orthomosaic derived from the UAV surveys is also presented with beach contour lines and levels in white. Image brightness and contrast are enhanced to visually differentiate gravels from sands (g, n).

A clear tidal stage relationship was evident in the process of cusps returning to the beach (Figure 13). That is, the main broad-scale beach response was one of lower beach accretion over the rising tides, and lower beach erosion on the falling tides. For the emergent cusp horn (Figure 13, Profile B), we observed significant lower beach (> 40 m cross-shore) accretion on the flood tides, with this sediment then reworked and consolidated into mid/upper beach horns (~ 40 m cross-shore) during the falling tides. When the flood tide and ebb tide morphological response is summed over the observation period, it is clear to see that the emergent horn grew most significantly on the ebb tides, accounting for 0.25 m of vertical growth at 29 m cross-shore, but also experienced net positive growth (0.1 m) on the flood tides at 27 m cross-shore (Figure 14). This is in direct contrast to the bay profile which eroded strongly on flood tides (0.25 m) and was largely stable on ebb tides

over the observation period. At lower beach locations (> 35 m cross-shore), both profiles experienced comparable magnitudes of erosion on the ebb tides and accretion on the flood tides.

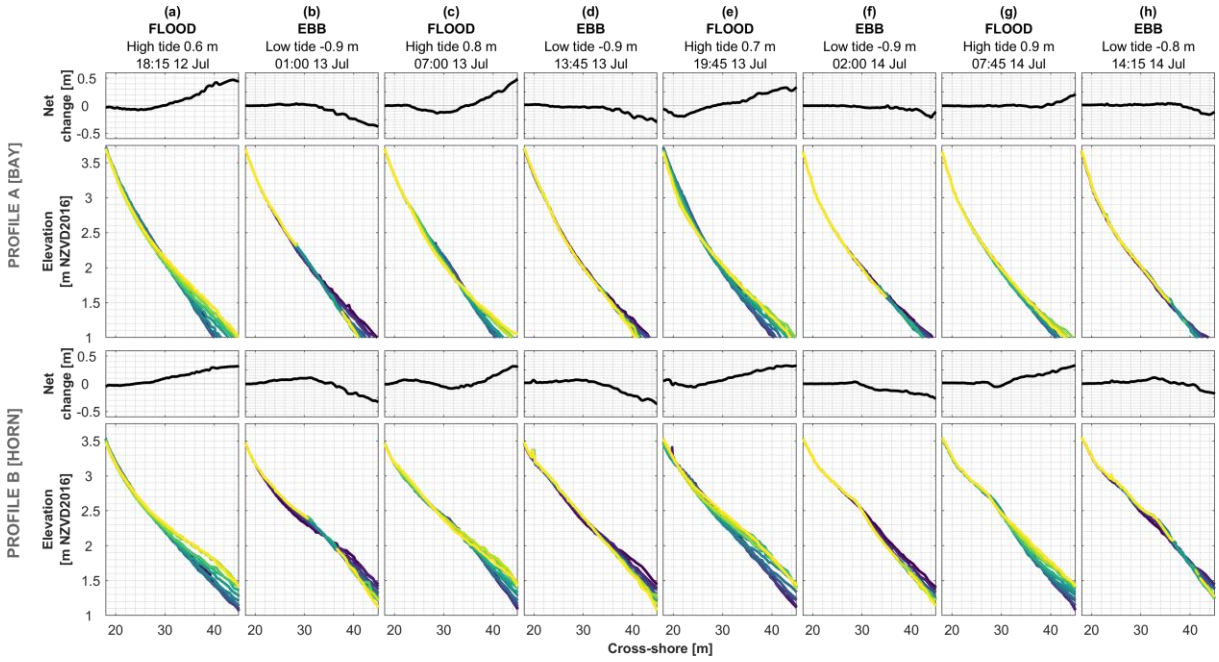

Figure 13. Beach topographic change at 30 minute intervals during individual flood and ebb tides between 12th and 14th July. The beach profile change is represented by the individual profile lines, with darker colours (blues) representative of the profile at the beginning of the current flood or ebb tide, and lighter colours (yellow and green) representing the most recent profile at the end of that flood or ebb. Net morphological change over the entire tide is shown in the black line above each panel. Profile A represents a LiDAR profile across a developing bay in front of Tower 1, and Profile B represents a developing horn in front of Tower 2 (Figure 1b).

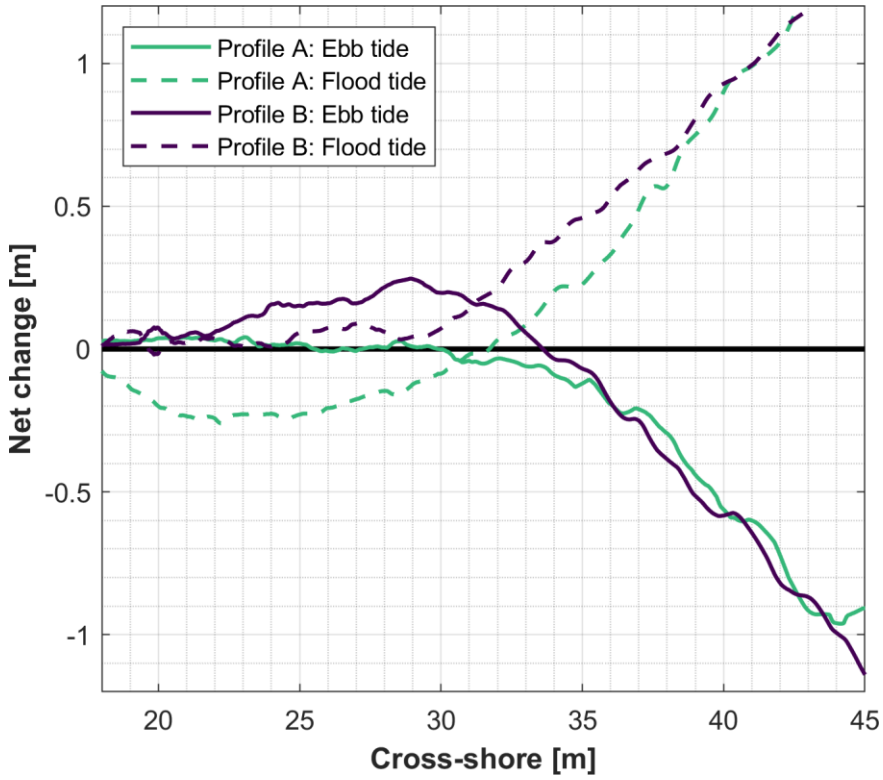

Figure 14. Tidally averaged changes observed for Profiles A and B between the 12th and 14th July (the period shown in Figure 13). Cumulative change observed over ebb tides for each profile is shown as a solid line, and cumulative flood tide morphological change is shown as a dashed line. The trend broadly is for lower beach elevations to experience erosion on ebb tides, and accretion on flood tides, with a more of a mixed response in the mid beach area.

4 Discussion

4.1 Cusp formation

4.1.1 Mixed sediment dynamics

Following the peak of the storm during Event 1 we observed rapid re-emergence of cusp horns on the lower beach, with a field of irregularly spaced and sized horns forming over the course of one ebb tide, and the bulk of the geomorphological adjustment taking place within 2.5 hours. This rapid formation was facilitated by the removal of surficial gravels on the mid beach by storm

action, exposing the relatively impermeable sandy substratum (Figure 6d). The darkest pixel imaging method in the current study was a novel method to show this transition as the associated changes in hydraulic conductivity exhibit a clear visual signature. Subsequently, as wave conditions waned, onshore transport was initiated and coarse gravels began to return to the beach where they were rapidly worked into horns. Longuet-Higgins and Parkin (1962) observed that coarse sediments (gravels) overlying a sandy substrate were highly mobile and thus could readily be reworked into horns. Using painted pebbles, they observed cusp formation to occur after the pebbles had been transported offshore into the surf zone as they subsequently returned and were deposited on cusp horns. This differs slightly from the conceptual pathway detailed in Guest and Hay (2019), where the same rapid transportability of gravels overlaying sand was observed, but in their case the gravel in the swash zone was reworked into horns, rather than first being removed offshore. Some useful insight is provided by Daly et al. (2021) who use XBeach modelling to look at the morphodynamic behaviour of varying sediment fractions during cusp formation on a sand beach. Their observation is that generally, finer material is moved offshore into the surf zone, and coarser sediments armour the swash zone. The lateral segregation of coarser and finer sediments into horns and bays is noticeably more pronounced on the falling tide. In the current study, our observations appear to lend support for this armouring of the swash zone, specifically when we examine the dynamics of horn emergence at the end of Event 1. We see in video imagery (Figure 6) that lateral sorting is extremely expeditious as the visual signature of hydraulic conductivity develops into well-defined rhythmic features in timescales of 1 to 2 hours. Furthermore, the LiDAR beach profile data provides evidence for contemporaneous erosion of the bay and accretion of the horn, which is indicative of coarser sediments being transported to the horns. This process was also observed by Guest and Hay (2019) whom noted that on mixed sediment beaches

experiencing cusp emergence: (1) coarser grains are preferentially deposited on areas of high relief; (2) this reduces transport capacity on the emergent horns due to lower fluid velocity; (3) interlocking and infiltration on the horns provide a positive feedback mechanism for more coarse deposition; and (4) coarse material remaining in the bays is more readily transported due to less bed friction. Positive feedback loops play an integral role in the rapidity of morphological change observed here. Masselink and Li (2001) found 1.5 mm to be a critical sediment size threshold above which infiltration through sediment contributed to significant profile steepening through onshore swash asymmetry. As coarse sediments begin to accumulate on the horns, this infiltration increases deposition through a reduced backwash volume (Dodd et al., 2008), especially when in comparison to the impermeable sandy substrate that begins to form the bays, which is the signature shown in Figure 6.

We found a much slower response time during Event 2 which occurred under lower wave conditions and with lower tidal water levels. Here, at the onset of the event gravel was distributed throughout the profile but it was not immediately reworked into horns. Instead, as maximum tidal elevations increased over the course of the event the gravels were progressively consolidated towards the upper beach. As tidal height and run up increased between the 5th and 6th July, alongshore segregation of sediments became most pronounced and coincided with the emergence of regular cuspate morphology. The formation of cusps, albeit not well developed, mid way through Event 2 (in the absence of prominent alongshore sorting of sediment), contrasts the predominant observations of cusps on mixed sediment beaches that show strong tendencies for lateral sorting of gravels into horns and sand into bays (Guest and Hay, 2019; Matsumoto et al., 2020). However, we note this does reflect the form the beach exhibited by the end of Event 2. In the current analysis, we were only able to apply a qualitative judgement as to whether the surficial

sediments were sand or gravel based on the orthophotos, and therefore are unable to quantify whether any sorting within the gravel segment was present such that smaller gravels occupied the bays.

4.1.2 Timescales

Timescales of cusp formation were many and varied over the course of the experiment. The 6 hours on the back of Event 1 represents a rapid transition from planar beach to developed cusps. At the end of the experiment cusp formation was much more prolonged, with the initial emergence of cuspate morphology over the course of 12 hours but requiring a full 24 hours to develop into a prominent, regularly spaced and well-defined cusp field. Two studies from the Field Research Facility at Duck, North Carolina, provided useful insight into cusp formation timescales. Utilising years of Argus imagery, Holland (1998) noted that transition from planar beach to well-developed cusp fields typically took a number of days. At the same location, O'Dea and Brodie (2019) investigated the emergence of rhythmic topography in a series of low tide LiDAR-derived elevation models. Their results demonstrate the emergence of well-developed cusps between consecutive low tides (~12 hours), with around 0.3 m cusp amplitude and 4 m cusp depth developing in that time. Guest and Hay (2019) noted that for a mixed sand-gravel beach (Advocate, Nova Scotia) the timescales required to destroy relict cusp morphology and for the re-emergence of new morphology with a different wave length could be on the order of 10s of minutes up to an hour, typically centred around high tide. This rapid timescale, compared to our present study, is likely explained by the different sedimentological composition. Advocate is mixed sand-gravel, meaning that under most conditions the beach matrix remains well mixed and co-located, and therefore the beach face readily contains ample proportions of both sand and gravel for hydraulic sorting into cusps to occur. Conversely, on a composite beach, a combination of processes needs

to occur to transport sediment cross-shore before longshore sorting resulting in cusp emergence can take place. For example, we observed the requirement for gravels to first be reintroduced to the lower beach face after storm activity, where an otherwise sandy substrate existed.

The varying timescales observed in the current study could be further considered in terms of wave energy. The rapid formation of cusps on one falling tide during Event 1 was during a high wave energy ($H_s \approx 2.5$ m) event, whereas the prolonged formation over a number of days in Event 3 took place whilst wave heights were typically 1.5 m. This is in agreement with a study by Coco et al. (2000) where increased sediment transport potential (for example, under higher wave conditions) was shown to be a primary control on the rate at which beach cusps were able to form, expressed in terms of the number of swash cycles required for cusp morphology to emerge. One other key difference between these two events is the relative regularity of the emerging bedforms. Cusp formation post-storm (Event 1) did not display the classical rhythmic spacing normally expected of beach cusps, but instead took the form of irregular isolated horns that had different spacings and depths (Figure 4c). The locations in which cusp horns did reform correlate to areas on the upper beach where the suppressed remnants of cusp horns appear to remain, in the form of offshore deviation in the contour lines. This implies that antecedent morphology exerted a large degree of control over the process of cusp formation, and the rapid (< 6 hours) development of the cusps following this event confirms that positive feedback exploiting existing morphological irregularities is a highly efficient and expeditious process (Masselink et al., 1997). Thus, high wave energy and therefore high sediment transport potential is not alone enough to initiate rapid cusp formation, else cusp re-emergence would be more uniform. In Coco et al's. (2000) study, they comment that the rate of initial formation was highly variable and largely dependent on the random

initial seeding of morphology in their model which exerted a greater control than sediment transport potential alone.

4.1.3 Tidal controls

Broadly, the lower beach accreted over the rising tide and eroded over the falling tide. When considering the role of tides in moderating cuspate morphology, Coco et al. (2004) noted that beach cusp morphology is less evident after the rising tide due to higher magnitude embayment accretion, and conversely, cusps are more prominent on the falling tide due to preferential erosion in the embayments. In the current study we also observe cusps emerging on the falling tide, but Event 1 shows a distinctly different mechanism for this change. Although we do see significant erosion in the bay, we also observe accretion of a comparable magnitude on the horns, such that overall beach volume averaged between the two profiles is approximately conserved. We attribute this to the mixed sediment nature of the site as outlined above, which also mirrors the study of Guest and Hay (2019) who also describe horn accretion occurring contemporaneously with embayment erosion on the falling tide. Much of the change associated with this horn emergence was concentrated within the first 2.5 hours after high tide when tidal translation rates were lowest and energy was focussed at a discrete cross-shore portion of the profile. This contrasts the findings of Masselink & Pattiaratchi (1998) who reported early falling tidal stages as important in emplacing new cusps, but latter falling tidal stages responsible for consolidation and growth. Given that Amberley is a composite beach, low tide conditions normally mean much energy is dissipated across the shallow gently sloping lower beach, whereas at or near high tide, the beach is more likely to be reflective in nature and subject to higher wave energy (Jennings and Shulmeister, 2002). Therefore, tidal elevation exerts a large degree of control on the amount of energy able to reach the lower and mid beach, and thus the sediment transport potential for cusp formation. This

also goes some way to explaining the persistence of mid beach accretion in Profile B during Event 3, where the focus of this accretion is the location where the lower beach sandy profile transitions into gravels through the upper and mid beach.

4.2 Changes in cusp spacing

We demonstrate that cusp adjustment is non-uniform along the beach face. During Event 2, the lesser developed northern section of the study area showed a reduction in wavelength as new cusp horns developed and a more regular and rhythmic topography emerged, whereas in the southern section which was already comparatively more regular, cusp spacing increased through the removal of interspersed horns. Further, during Event 3 the northern part of the beach showed a significant adjustment through the reduction of cusp spacing whereas the southern part remained largely unchanged. This is commensurate with a number of studies that highlight self organisation as a key driver of cusp formation, where initial perturbations in the beach face are irregular in size and spacing, and gradually become more regular over progressive swash cycles (Coco et al., 2000; Werner and Fink, 1993). In the present study, this occurs during Event 2 as run up height is predicted to increase as a function of increased wave height, resulting in a higher sediment transport potential and thus a reduced morphodynamic response time, as well as increased potential to transport eroded coarse sediments from the surf zone back onto the beach. In the southern part of the beach, where intermediate horns are removed, we are likely to see that this increase in swash excursion results in overtopping of horns rather than a more typical horn-divergent flow regime, which ultimately increases the spacing (Masselink et al., 1997). In the northern part, as areas of high relief emerge and divert swash flow towards areas of lower relief, positive feedback inhibits the growth of other horns. We therefore observe the survival and amplification of morphodynamic perturbations that are spaced far enough away from the inhibitory (erosive) effect of neighbouring

emergent bedforms (Murray et al., 2020), resulting in the transition from a relatively planar beach towards a cuspate form, and therefore the observed reduction in the spacing between horns. This observation is important as typically field observations of either merging (Almar et al., 2008) or destruction of intermediate features (Masselink et al., 1997) tend to demonstrate a more alongshore-uniform process, rather than divergent responses in proximal locations. During Event 3, run up height reduced and this in turn led to two new horns emerging and the overall reduction in cusp spacing. As swash width decreases, the magnitude of alongshore (bay-orientated) flow deflection from the horns is decreased, meaning the erosive power associated with the backwash from horn divergent flows becomes more localised to the existing horns. This creates a relative low energy zone between horns that is not subject to the erosive backwash and thus emerges as a localised area of high relief, initiating positive feedback between flow and morphology and allowing a new cusp horn to develop.

5 Conclusions

The in situ deployment of two LiDAR towers were combined with daily low tide topographic surveys over a three week period to better understand cusp morphodynamics on a composite beach. The key finding is that movement of coarse sediment around the system exert a primary control on the timescales of beach cusp formation, with our observations showing highly mobile storm-eroded gravels were rapidly (< 3 hours) reworked into prevalent horns during the waning stages of a storm. The mixed sediment matrix (gravels versus sand) was shown to exert a strong degree of control on this process, with coarse gravels shown to be highly mobile across a comparatively impermeable sandy substrate, accounting for the rapid reformation of cusps.

We observe alongshore irregularity in cusp return as a result of feedback mechanisms between morphology, sediment characteristics, and flow. We provide the first field evidence of cusp spacing adjustment taking place through divergent modes, whereby some areas of the beach experience destruction of intermediate horns whilst other simultaneously experience growth of new emergent horns as the entire beach adjusts from antecedent imprints to the new forcing conditions. The timescales of cusp return appear to be controlled by both the relative separation and availability of sediment types (sand and gravel), and also by the sediment transport potential of the incident wave field, with higher wave conditions observed to result in the most expeditious cusp building episode. The composite nature of the beach and the associated difference in gradient between the gently sloping lower and steeper upper beach appears to regulate wave energy required for cusp formation across the course of a tidal cycle, and given the right conditions allow cusp horn growth to take place across both the rising and falling tidal stages.

Given the clear controls exerted by sedimentology evident here, future work should focus on the precise dynamics of the sand-gravel interaction. We demonstrated that coastal imaging products such as darkest pixel are potentially a powerful method of quantifying this process through the visualisation of infiltration, but note that this only provides evidence of the surface composition of sediments, and provides no information on the vertical structure.

Acknowledgments

We are extremely grateful for three thorough and insightful anonymous reviews which significantly improved the scope and depth of this research. The authors would like to thank Paul Bealing, Justin Harrison, Nick Key and Pete Wilson for support with the development and

deployment of the field gear. We are thankful for funding from the Brian Mason Scientific and Technical Trust that enabled this fieldwork to go ahead, and for support from Justin Cope and Bruce Gabites at Environment Canterbury in the lead up to the experiment.

References

Ali, S., Darsan, J., Wilson, M., 2017. Cusp morphodynamics in a micro-tidal exposed beach. Journal of Coastal Conservation 21, 777–788. https://doi.org/10.1007/s11852-017-0536-2

Almar, R., Coco, G., Bryan, K.R., Huntley, D.A., Short, A.D., Senechal, N., 2008. Video observations of beach cusp morphodynamics. Marine Geology 254, 216–223.

Almeida, L.P., Masselink, G., Russell, P.E., Davidson, M.A., 2015. Observations of gravel beach dynamics during high energy wave conditions using a laser scanner. Geomorphology 228, 15–27. https://doi.org/10.1016/j.geomorph.2014.08.019

Buscombe, D., Masselink, G., 2006. Concepts in gravel beach dynamics. Earth-Science Reviews 79, 33–52. https://doi.org/10.1016/J.EARSCIREV.2006.06.003

Byun, D.-S., Hart, D.E., 2020. A monthly tidal envelope classification for semidiurnal regimes in terms of the relative proportions of the the S2, N2, and M2 constituents. Ocean Sci. 16, 965–977. https://doi.org/10.5194/os-16-965-2020

Coco, G., Burnet, T.K., Werner, B.T., Elgar, S., 2004. The role of tides in beach cusp development. Journal of Geophysical Research 109, C04011. https://doi.org/10.1029/2003JC002154

Coco, G., Burnet, T.K., Werner, B.T., Elgar, S., 2003. Test of self-organization in beach cusp formation. Journal of Geophysical Research: Oceans 108. https://doi.org/10.1029/2002jc001496

Coco, G., Huntley, D.A., O'Hare, T.J., 2000. Investigation of a self-organization model for beach cusp formation and development. Journal of Geophysical Research: Oceans 105, 21991–22002. https://doi.org/10.1029/2000jc900095

Coco, G., Murray, A.B., 2007. Patterns in the sand: From forcing templates to self-organization. Geomorphology 91, 271–290. https://doi.org/10.1016/j.geomorph.2007.04.023

Coco, G., O'hare, T.J., Huntley, D.A., 1999. Beach Cusps: A Comparison of Data and Theories for Their Formation, Source: Journal of Coastal Research.

Daly, C.J., Floc'h, F., Almeida, L.P.M., Almar, R., Jaud, M., 2021. Morphodynamic modelling of beach cusp formation: The role of wave forcing and sediment composition. Geomorphology 389, 107798. https://doi.org/10.1016/j.geomorph.2021.107798

Dodd, N., Stoker, A.M., Calvete, D., Sriariyawat, A., 2008. On beach cusp formation. Journal of Fluid Mechanics 597, 145–169. https://doi.org/10.1017/S002211200700972X

Guest, T.B., Hay, A.E., 2019. Timescales of beach cusp evolution on a steep, megatidal, mixed sand-gravel beach. Marine Geology 416, 105984. https://doi.org/10.1016/j.margeo.2019.105984

Guza, R.T., Inman, D.L., 1975. Edge waves and beach cusps. Journal of Geophysical Research 80, 2997–3012. https://doi.org/10.1029/jc080i021p02997

Hart, D.E., Marsden, I.E., Francis, M., 2008. Coastal Systems, in: Winterbourne, M., Knox, G., Burrows, C., Marsden, I.E. (Eds.), The Natural History of Canterbury. pp. 653–684.

Holland, K.T., 1998. Beach cusp formation and spacings at Duck, United States. Continental Shelf Research 18, 1081–1098. https://doi.org/10.1016/S0278-4343(98)00024-7

Holland, K.T., Holman, R., 1996. Field observations of beach cusps and swash motions. Marine Geology 134, 77–93. https://doi.org/10.1016/0025-3227(96)00025-4

Holman, R., Stanley, L., 2007. The history and technical capabilities of Argus. Coastal Engineering 54, 477–491.

Horn, B., 1987. Closed-form solution of absolute orientation using unit quaternions. J. Opt. Soc. Am. A 4, 629. https://doi.org/10.1364/JOSAA.4.000629

Horn, D., Walton, S.M., 2007. Spatial and temporal variations of sediment size on a mixed sand and gravel beach. Sedimentary Geology 202, 509–528. https://doi.org/10.1016/j.sedgeo.2007.03.023

Jennings, R., Shulmeister, J., 2002. A field based classification scheme for gravel beaches. Marine Geology 186, 211–228. https://doi.org/10.1016/S0025-3227(02)00314-6

Longuet-Higgins, M.S., Parkin, D.W., 1962. Sea Waves and Beach Cusps. The Geographical Journal 128, 194. https://doi.org/10.2307/1793470

Masselink, G., 1999. Alongshore variation in beach cusp morphology in a coastal embayment. Earth Surface Processes and Landforms 24, 335–347. https://doi.org/10.1002/(SICI)1096-9837(199904)24:4<335::AID-ESP968>3.0.CO;2-H

Masselink, G., Hegge, B.J., Pattiaratchi, C.B., 1997. Beach cusp morphodynamics. Earth Surface Processes and Landforms 22, 1139–1155. https://doi.org/10.1002/(SICI)1096-9837(199712)22:12<1139::AID-ESP766>3.0.CO;2-1

Masselink, G., Li, L., 2001. The role of swash infiltration in determining the beachface gradient: a numerical study. Marine Geology 176, 139–156. https://doi.org/10.1016/S0025-3227(01)00161-X

Masselink, G., Pattiaratchi, C., 1998. Morphodynamic Impact of Sea Breeze Activity on a Beach with Beach Cusp Morphology. Journal of Coastal Research 14, 393–406.

Matsumoto, H., Young, A.P., Guza, R.T., 2020. Cusp and Mega Cusp Observations on a Mixed Sediment Beach. Earth and Space Science 7, e2020EA001366. https://doi.org/10.1029/2020EA001366

Murray, B., Ashton, A.D., Coco, G., 2020. From cusps to capes: self-organised shoreline shapes, in: Jackson, D., Short, A. (Eds.), Sandy Beach Morphodynamics. Elsevier, pp. 277–295. https://doi.org/10.1016/b978-0-08-102927-5.00012-6

Nolan, T.J., Kirk, R.M., Shulmeister, J., 1999. Beach cusp morphology on sand and mixed sand and gravel beaches, South Island, New Zealand. Marine Geology 157, 185–198. https://doi.org/10.1016/S0025-3227(98)00150-9

O'Dea, A., Brodie, K.L., 2019. Spectral analysis of beach cusp evolution using 3D LiDAR scans, in: Coastal Sediments 2019. Presented at the International Conference on Coastal Sediments 2019, WORLD SCIENTIFIC, Tampa/St. Petersburg, Florida, USA, pp. 657–673. https://doi.org/10.1142/9789811204487_0058

Otvos, E.G., 1964. Observation of Beach Cusp and Beach Ridge Formation on the Long Island Sound. SEPM Journal of Sedimentary Research Vol. 34. https://doi.org/10.1306/74D710EB-2B21-11D7-8648000102C1865D

Pitman, S., Hart, D.E., Katurji, M., 2019a. Beach cusp morphodynamics on a composite beach observed using UAV structure from motion, in: Proceedings of the Australasian Coasts & Ports Conference. Hobart, Tasmania.

Pitman, S., Hart, D.E., Katurji, M.H., 2019b. Application of UAV techniques to expand beach research possibilities: A case study of coarse clastic beach cusps. Continental Shelf Research. https://doi.org/10.1016/j.csr.2019.07.008

Poate, T.G., Masselink, G., McCall, R.M., Russell, P.E., Davidson, M.A., 2014. Storm-driven cusp behaviour on a high energy gravel beach. Journal of Coastal Research 70, 645–650. https://doi.org/10.2112/SI70-109.1

Poate, T.G., McCall, R.T., Masselink, G., 2016. A new parameterisation for runup on gravel beaches. Coastal Engineering 117, 176–190. https://doi.org/10.1016/J.COASTALENG.2016.08.003

Sallenger, A.H., 1979. Beach-cusp formation. Marine Geology 29, 23–37. https://doi.org/10.1016/0025-3227(79)90100-2

Sherman, D.J., Orford, J.D., Carter, R.W.G., 1993. Development of cusp-related, gravel size and shape facies at Malin Head, Ireland. Sedimentology 40, 1139–1152. https://doi.org/10.1111/j.1365-3091.1993.tb01384.x

van Gaalen, J.F., Kruse, S.E., Coco, G., Collins, L., Doering, T., 2011. Observations of beach cusp evolution at Melbourne Beach, Florida, USA. Geomorphology 129, 131–140. https://doi.org/10.1016/J.GEOMORPH.2011.01.019

Werner, B.T., Fink, T.M., 1993. Beach cusps as self-organized patterns. Science 260, 968–971. https://doi.org/10.1126/science.260.5110.968